Buddy Routing: A Routing Paradigm for NanoNets Based on Physical Layer Network Coding

Ruiting Zhou[†], Zongpeng Li [†‡], Chuan Wu [§], Carey Williamson[†]

[†] Department of Computer Science, University of Calgary, Canada

[‡] Institute of Network Coding, The Chinese University of Hong Kong

[§] Department of Computer Science, The University of Hong Kong

Abstract— **NanoNets are networks of nanomachines at extremely small dimensions, on the order of nanometers or micrometers. Recent advances in physics and engineering have made basic computing and communication feasible on nanomachines, and NanoNets are envisioned as an important emerging technology with broad future applications. Traditional networking solutions require significant modifications for application in NanoNets. In this paper, we focus on routing algorithm design in NanoNets. Based on the salient features of a NanoNet, including low node cost and very low available power, we propose a new routing paradigm for unicast and multicast data transmission in NanoNets. Our design, termed** *Buddy Routing (BR)*, **is enabled by latest advancements in physical layer network coding, and argues for pair-to-pair data forwarding in place of traditional node-to-node data forwarding. Through both analysis and simulations, we compare BR with point-to-point routing, in terms of raw throughput, error rate, energy efficiency, and protocol overhead, and show the advantages of BR in NanoNets.**

I. INTRODUCTION

NanoNetworks represent an emerging type of wireless sensor networks consisting of nanonodes — wireless nodes at extremely small form factors, on the order of micrometers or nanometers. This work aims to present the first routing/MAC protocol design tailored for multi-hop NanoNets, by utilizing physical layer network coding (PNC) for pair-to-pair routing that break through the frugal nodal power limitation at nanonodes.

As shown in Fig. 1, the structure of a nanonode resembles that of a wireless sensor node to a great extent. Recent advances in physics and engineering technologies have made it possible to manufacture storage, processor, radio antenna and power supply at the nano-scale [1], [2]. For example, a typical nanotube based transmitter has a volume of $3.9 \times 10^4 \ nm^3$ [3]. Electromagnetic communication between nanonodes can be enabled by either frequency modulation or phase modulation. Such invisibly small nanonodes can be easily attached to everyday objects or human bodies, for sensing antigen molecules, the immune system, or other physical parameters of interest.

Compared with a wireless mesh network and a 'regular' wireless sensor network, a NanoNet has a number of salient features. Nanotube radiation is at Terahertz domain, leading to wavelengths on the order of 0.1 mm, and usually travels in line-of-sight fashion. Nano-processors, nano-tranceivers and nano-power supply are usually of orders of magnitude weaker than their counterparts in wireless mesh networks. Due to limitations in nano-battery technologies, power supply is weak and short-lived, *e.g.*, providing current at $45\mu A$ per $cm^2 \cdot \mu m$, and requir-
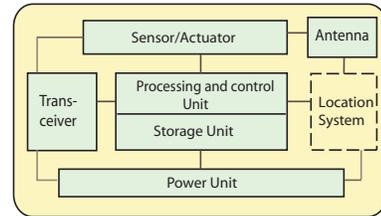
Fig. 1. The architecture of a nanonode.

ing periodical recharges [1], [4]. Consequently, direct nano communication can only happen in very short distances, and at very low rates. In short, NanoNets present an entirely new networking paradigm that invites radical revolutions in networking solutions, including error detection/correction, routing and MAC algorithms [5].

By grouping nodes into collaborating pairs, pair-to-pair forwarding can breakthrough the fundamental nodal power constraint, enhancing the communication range and rate of nanonodes, and is therefore a promising paradigm for exploration in routing algorithm design for NanoNets. Such routing algorithms are best coupled with a simple MAC algorithm, such as TDMA, so that execution on nano processors does not become a bottleneck.

Collaborative data forwarding among paired nanonodes can be enabled by two different physical layer techniques: amplify&forward (A&F), or physical layer network coding (PNC) [6]. A detailed comparison between the two, in terms of error rate and capacity, is provided in Sec. II. We choose PNC for its potential in higher communication rate. PNC is a recent technology that views the overlap of analog signals in the air as linear combination of source signals. PNC based mapping and demodulation can be applied to decode for a digital version of the linear combination [6], [7].

Fig. 2 illustrates how PNC can enable pair-to-pair data forwarding that underlies our proposal of Buddy Routing (BR). Assume the source packet x for transmission is broken into two equal-length sub-packets x_1 and x_2. We pair up each of the Tx node and Rx node with a nearby 'buddy' node. The Tx node shares x_1 with its buddy, through a short intra-pair transmission. Next, the two Tx nodes simultaneously transmit x_1 and x_2 respectivvely to the two Rx nodes, such that their signals are aligned at the buddy node ($N1$) in the Rx pair, which performs PNC to demodulate $x_1 + x_2$, and forwards it to the Rx node
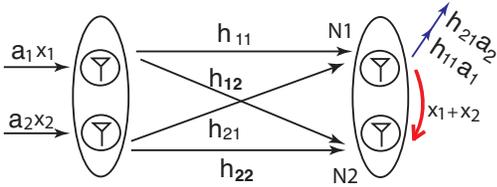
Fig. 2. Pair-to-pair based buddy forwarding enabled by PNC. Precoding is performed at the Tx pair, for signal alignment at N1: $h_{11}a_1 = h_{21}a_2$. Here h_{ij} is a complex number charactering channel fading from a node in the Tx pair to a node in the Rx pair, which includes amplitude attenuation and phase shift.

($N2$). The Rx node can recover the original packet x from the analog signal it receives, $h_{12}a_1x_1 + h_{22}a_2x_2$, and the encoded packet from its buddy, $x_1 + x_2$, e.g., through an adapted version of Maximum-Likelihood (ML) decoding [7]. Higher communication rate is targeted for data sharing within each pair, with a higher modulation rate. For example, BPSK modulation can be applied for the inter-pair transmission, and 16QAM for intra-pair.

Our main proposal, Buddy Routing (BR), is a PNC-enabled pair-to-pair routing solution, coupled with a tailored and streamlined TDMA MAC for simplicity and efficiency. The design of BR targets both unicast and multicast applications. For the latter, a multicast gadget enabled by PNC will be designed and utilized (Sec. V, Fig. 16). We design and present the pipeline operation for data forwarding along a BR route. Through theoretical analysis, we obtain insights on the effect of key parameter selection on the performance of BR. We extend the geographical greedy routing algorithm [8] to its pair-to-pair forwarding version, for computing a BR unicast route. Iterative MAC layer optimization, over both Tx power at nanonodes and lengths of time slots in the TDMA MAC are refined, for mitigating bottleneck interference and end-to-end capacity improvement. Simulation results verify the theoretical analysis that BR has a potential to substantially improve the end-to-end throughput of traditional point-to-point routing.

We further extend the solution design from multi-hop unicast to multi-hop multicast, by designing a pair-forwarding based multicast tree construction algorithm, and adapting the iterative MAC optimization algorithm from a unicast path to a multicast tree. A two fold increase in multicast throughput is observed in large scale network simulations.

To our knowledge, BR represents the first multi-hop routing algorithm design for NanoNets, as well as the first such algorithm that leverages PNC in collaborative multi-hop routing. We believe that BR has a potential to breakthrough the power supply bottleneck in NanoNets and *smart dust* [9] that are formed of extremely small and extremely weak wireless nodes, especially when coupled with a simple and efficient MAC protocol, such as TDMA.

II. ENABLING BUDDY ROUTING: PNC *vs.* AMPLIFY&FORWARD

The pair-to-pair forwarding gadget depicted in Fig. 2, underlying the idea of Buddy Routing, can be enabled by either PNC or Amplify&Forward (A&F). A number of virtual MIMO forwarding schemes recently proposed are in essence based on A&F-enabled collaboration [10], [11]. The main difference between

PNC and A&F lies in the intra-pair transmission to the Rx node from its buddy: in PNC, the Tx buddy transmits a digital version of $x_1 + x_2$; in A&F, it transmits an amplified version of the received analog signal $h_{11}a_1x_1 + h_{21}a_2x_2$.

In this section, we compare these two enabling technologies in terms of multi-hop throughput potential (II-A), single-hop BER (II-B), and protocol overhead.

A. PNC vs. A&F: Multi-hop Buddy Routing
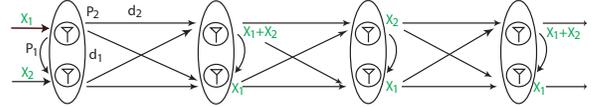
Fig. 3. BR transmission in a multi-hop unicast route enabled by PNC

Fig. 3 shows the pipeline operation of a multi-hop route based on pair-to-pair forwarding, enabled by PNC. Except at the source pair, there is no need for half-packet sharing in subsequent buddy pairs for subsequent pair-to-pair transmission. The top receiver has already demodulated a digital half-packet (labeled in figure) that can be directly used. As a result, all short hop (intra-pair) transmissions can happen simultaneously along the entire BR route, without incurring severe interference.
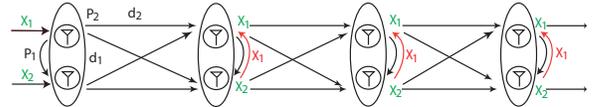
Fig. 4. BR Transmissions in a multi-hop unicast route enabled by A&F.

In contrast, Fig. 4 depicts the pipeline operation of a BR route enabled by A&F. We highlight that, in order to prepare for the pair-to-pair transmission, intra-pair sharing of a half-packet is required at each hop. This is an extra step of transmission that does not exist in the PNC-enabled BR route. As a result, an extra time slot is required for scheduling such intra-pair half-packet sharing, leading to a lower end-to-end data throughput.

B. PNC vs. A&F: One-hop BER

We first analyze the BER performance of PNC, and then compare with the BER of A&F. We ignore the BER for the Tx node to share x_1 with its buddy, since it is the same for both schemes, and is relatively small, due to the short distance.

1) BER of PNC: For the one-hop gadget in Fig. 2, the BER performance of PNC can be analyzed in two phases. In phase one, we study the BER at $N1$, for decoding $x_1 + x_2$. In phase two, we study the BER at $N2$ for decoding x_1 and x_2, assuming an adapted version of Maximum-Likelihood (ML) detection [7].

BER at $N1$. $N1$ can demodulate $x_1 + x_2$ by applying ML detection and PNC mapping. Let $\mathbf{c} = x_1 + x_2$ which is in the $\{-2, 0, 2\}$ domain according to PNC mapping under BPSK modulation. Let $\mathbf{c_i}$ and $\mathbf{c_k}$ be two possible transmit vectors, with $i, k \in \{1, 2, 3\}$ being indices to $\{-2, 0, 2\}$. Assume $\mathbf{c_i}$ is received, the probability that $N1$ incorrectly outputs $\mathbf{c_k}$ is:

$$Pr(\mathbf{c_i} \rightarrow \mathbf{c_k}) = Q\left(\sqrt{\frac{d_{ik}^2}{2\sigma_{PNC-SA}^2}}\right) = Q\left(\sqrt{\frac{\lambda_{ik}\rho_1}{2}}\right),$$

where $\lambda_{ik} = (\mathbf{c_i} - \mathbf{c_k})^T(\mathbf{c_i} - \mathbf{c_k})$, and ρ_1 is the received SNR at N1. Function Q computes the area under the tail of a Gaussian PDF.

The ternary values in $\{-2, 0, 2\}$ appear in $\mathbf{c}$ with probabilities of: $\mathbf{c_1} = -2 : 25\%$, $\mathbf{c_2} = 0 : 50\%$, $\mathbf{c_3} = 2 : 25\%$, assuming 0 and 1 are equally possibile to appear in the original data packet. $Pr(\mathbf{c_i} \to \mathbf{c_k}) = 0$ when both $\mathbf{c_i}$ and $\mathbf{c_k}$ are in $(\pm 2, \pm 2)^T$. In other words, judging -2 to be $+2$ or vice versa does not lead to an error in $x_1 + x_2$. N1 wishes to demodulate the digital bits $x_1 + x_2$. The average vector error probability, which is also the bit error rate, for $\mathbf{x_1} + \mathbf{x_2}$ is

$$Pr_s(x_1 + x_2) = Pr_b(x_1 + x_2)$$

$$= 2P(\mathbf{c_1})Pr(\mathbf{c_1} \to \mathbf{c_2}) + P(\mathbf{c_2}) \sum_{i \neq 2} Pr(\mathbf{c_2} \to \mathbf{c_i})$$

BER at $N2$. We apply adapted ML, a detection scheme tailored for collaborating PNC receivers recently proposed by us [7], to decode x_1 and x_2. Before applying the normal min-distance criterion in ML, it first filters out the enumerated vectors that are not in agreement with the known values for $x_1 + x_2$, to reduce the computational complexity. Using 16QAM modulation, there are 16 such vectors, with dimension 2×1. $\tilde{\mathbf{x}}_\mathbf{i}$ and $\tilde{\mathbf{x}}_\mathbf{k}$ are two distinct vector among the sixteen. Let Λ_c and Λ_w denote the events that N2 receives the correct and wrong data in $x_1 + x_2$ from $N1$, respectively. The average vector error probability when $x_1 + x_2$ is correct is

$$Pr_s(\tilde{\mathbf{x}}|\Lambda_c) = \frac{1}{16} \sum_{i=1}^{16} \sum_{k=1 k \neq i}^{16} Q\left(\sqrt{\frac{\lambda'_{ik}\rho_2}{10}}\right).$$

Here $\lambda'_{ik} = (\tilde{\mathbf{x}}_\mathbf{i} - \tilde{\mathbf{x}}_\mathbf{k})^T(\tilde{\mathbf{x}}_\mathbf{i} - \tilde{\mathbf{x}}_\mathbf{k})$, ρ_2 is the received SNR at node 2. In the constellation graph with ML decoding, when noise exceeds the decision threshold, only 1 bit will be in error. Thus, the approximate BER can be computed as

$$Pr_b(\tilde{\mathbf{x}}|\Lambda_c) \approx Pr_s(\tilde{\mathbf{x}}|\Lambda_c)/4$$

We next analyze the case that $x_1 + x_2$ transmitted from $N1$ contains error. We have $Pr_b(\tilde{\mathbf{x}}) = Pr_b(\tilde{\mathbf{x}}|\Lambda_c)Pr_b(\Lambda_c) + Pr_b(\tilde{\mathbf{x}}|\Lambda_w)Pr_b(x_1 + x_2)$. When information from $N1$ is wrong, $N2$ outputs a wrong vector with probability 1, $i.e., Pr_b(\tilde{\mathbf{x}}|\Lambda_w) = 1$. Therefore the vector error rate of the overall PNC-based scheme is

$$Pr_b(\tilde{\mathbf{x}}) = Pr_b(\tilde{\mathbf{x}}|\Lambda_c)(1 - Pr_b(x_1 + x_2)) + Pr_b(x_1 + x_2).$$

2) BER of Amplify&Forward: The analysis of BER performance for A&F with ML detetion is similar to that of a basic 2×2 MIMO link. $N2$ can decode x_1 and x_2 after receiving the amplified signal from $N1$. The vector error rate of A&F is:

$$Pr_s(A\&F) = \frac{1}{4} \sum_{i=1}^{4} \sum_{k=1 k \neq i}^{4} Q\left(\sqrt{\frac{\lambda''_{ik}\rho}{2}}\right),$$

where $\lambda'_{ik} = (\tilde{\mathbf{x}}_\mathbf{i} - \tilde{\mathbf{x}}_\mathbf{k})^T(\tilde{\mathbf{x}}_\mathbf{i} - \tilde{\mathbf{x}}_\mathbf{k})$, $\tilde{\mathbf{x}}_\mathbf{i}$ and $\tilde{\mathbf{x}}_\mathbf{k}$ are two possible spatial source vectors and $i, k \in \{1, \ldots, 4\}$. ρ is SNR at the receiver side. Then the BER of A&F can be approximated as:

$$Pr_b(A\&F) \approx Pr_b(A\&F)/2.$$

During joint ML decoding at $N1$, two SNR values are involved, the SNR for the pair-to-pair transmission, and the SNR to receive the amplified signal. Correspondingly, we plot two BER lines in the simulation: 'A&F-upper' assumes the pair-to-pair BER, 'A&F' assumes the average of the two SNR values.

3) Simulation result of BER : Fig. 5 shows the simulation results based on the BER analysis of PNC and A&F. We can observe that the BER of PNC is almost the same as but slightly worse than that of A&F, under the same SNR at the receiver side. A small price in BER is paid by the PNC scheme, for involving two steps of demodulation.
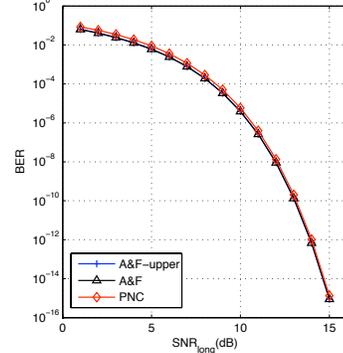
Fig. 5. PNC *vs.* virtual MIMO, ignoring error in collaborative steps.

To conclude, A PNC-enabled BR route and an A&F enabled BR route have comparable BER performance, while the former leads to a more efficient pipeline operation and a higher end-to-end throughput. In the rest of the paper, we focus on PNC as the enabling technology of BR routing. While the original proposal of PNC requires an extra overhead in symbol-level node synchronization, recent advances show that asynchronous PNC with only packet-level synchronization (required in the TDMA MAC underlying both PNC-based and A&F based schemes) can achieve similar performance, especially when channel coding is appropriately designed [12].

III. THEORETICAL ANALYSIS

A. System model and parameters

We consider a multi-hop BR route as shown in Fig. 6. Let $d_1 = \alpha d_2$, $P_1 = \beta P_2$. For ease of analysis, we assume in this section that the distance d_1 of each pair-to-pair hop is the same, and the inter-node distance d_2 is the same in each pair.

We can synchronize nodes in the network, and schedule two types of time slots: long slots and short slots. In each long time slot, the long hop pair-to-pair transmissions happen simultaneously every three hops, for mitigating interference (following the two-hop interference range in the protocol interference model [13]). Therefore, three long time slots are required: t_{11}, t_{12} and t_{13}. Every $(3k + 1)$-st long hop transmits in slot t_{11}, every $(3k + 2) - nd$ long hop transmits in slot t_{12}, and every $(3k + 3)$-rd long hop transmits in slot t_{13}. During short time slot t_2, all the intra-pair short hops transmit simultaneously.
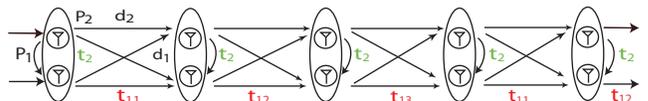
Fig. 6. BR System Model.

B. The Capacity of A BR Route

To analyze the end-to-end routing capacity of a BR route, we first compute SNR_{short} and SNR_{long}, BER values in the short and long transmissions, respectively.

Assume the path loss factor is 3, and the distance between a wireless Tx node and Rx node is d. Then the power available at the receiving antenna can be expressed by the power for the transmitting antenna and distance, which is $P_r = P_t/d^3$. Considering interference from immediate neighboring pairs along the BR path, the SNR of the short hop can be approximated as:

$$SNR_{short} = \frac{P_1/d_1^3}{\sigma^2 + 2 \times P_1/d_2^3} \qquad (1)$$

Here σ^2 is the intensity of additive white Gaussian noise. Considering interference from the closest two pairs that transmit concurrently in the BR TDMA scheme, the SNR of the long hop can be approximated as:

$$SNR_{long} = \frac{2 \times P_2/d_2^3}{\sigma^2 + 2 \times P_2/(2d_2)^3} \qquad (2)$$

According to the Shannon-Hartley Theorem, the capacity of a wireless link l is

$$C_l = B_l \log_2(1 + SNR_l),$$

where C_l is the channel capacity in bps and B_l is the bandwidth of the channel in hertz. The capacity of a k-hop BR route is the bottleneck capacity among all the long (inter-pair) and short (intra-pair) transmissions, at each hop i:

$$C_{BR} = \min\{C_{long-i}, C_{short-i} | 1 \leq i \leq k\}$$

Capacity at very high SNR. We first simulate the BR route capacity with noise ignored. Fig. 7 shows that the BR route capacity decreases when $d_1/d_2 > 0.39$. On the other hand, the ratio between P_1 and P_2 has no significant effect on the capacity. In this set of simulations, $B = 100KHz$, $P2 = 100\mu W$, $d_2 = 50$dm.

inter-pair transmissions. When $\alpha > 0.39$, the bottleneck becomes the intra-pair links, whose capacity decreases as d_1 increases.

Capacity with noise considered. We next simulate the capacity of a BR route with noise considered. Fig. 8 shows a decreasing trend of the BR route capacity as noise grows. In this set of simulations, noise intensity varies from 0 to $4 \times 10^{-6}W$, $P_2 = 100\mu W$, $d_2 = 50$dm, $d_1 = 5$dm. The bottleneck resides in the inter-pair transmissions, and changes in $\beta = P_1/P_2$ has no affect on capacity.
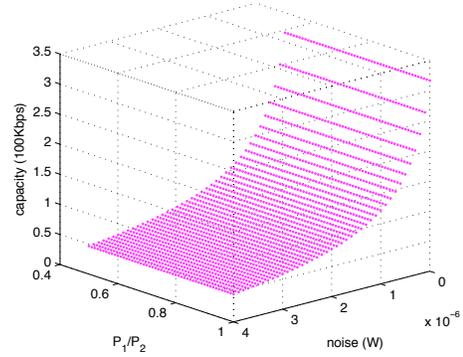
Fig. 8. Capacity with the effect of noise, $\alpha = 0.1$. BR route bottleneck exists in inter-pair transmissions, P_1/P_2 is irrelevant.

The short hop becomes a bottleneck when $SNR_{short} < SNR_{long}$. Substituting (1) and (2) into this inequality, we obtain the equivalent condition of

$$\sigma^2 < \gamma, \text{and } \alpha < (\frac{\beta}{2})^{1/3};$$

$$\text{or} \quad \sigma^2 > \gamma, \text{and } \alpha > (\frac{\beta}{2})^{1/3},$$

where $\gamma = \frac{(16-\alpha^{-3})\frac{P_2}{d_2^3}}{4\alpha^{-3} - \frac{8}{\beta}}$.

For the simulations in Fig. 9, σ^2 varies from 0 to $4 \times 10^{-7}W$, $P2 = 100\mu W$, $d_2 = 50$dm, $d_1 = 30$dm. Under such parameter settings, the bottleneck switches to the intra-pair links. Overall BR capacity decreases gradually as the noise level escalates.

Fig. 7. BR route capacity with different values for P_1/P_2 and d_1/d_2.

Without background noise, with constant P_2 and d_2, inter-pair link capacity is constant and does not depend on P_1/P_2. When $\alpha = d_1/d_2 < 0.39$, the bottleneck of the BR route lies in the
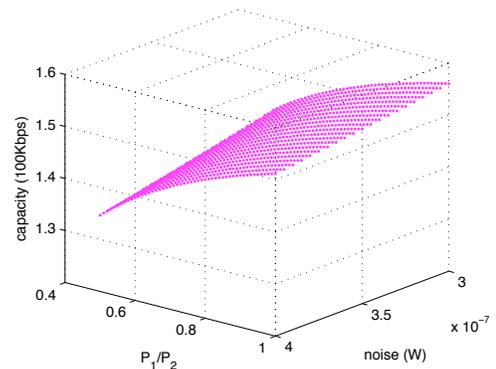
Fig. 9. Capacity with the effect of noise, $\alpha = 0.6$. BR route bottleneck exists in intra-pair links, P_1/P_2 is relevant.

From Fig. 9, we can see the as P_1 increases, the BR route capacity increases. However, for the same amount of information

routed, the total power consumption along the entire BR route increases. We therefore face a fundamental tradeoff between capacity and energy efficiency.

C. Power Consumption: BR vs. Point-to-Point Routing

Next, we compare the energy consumption, for routing the same amount information, between Buddy Routing and traditional point-to-point schemes. Again, we assume that BPSK and 16QAM are selected for modulation in the long and short BR transmissions, respectively. For point-to-point routing, a single node relays the data packet at each hop, using BPSK modulation. Let t be the time duration for one antenna to transmit one packet with BPSK modulation, and k be the number of (long) hops from the source to the destination. At each hop, the energy consumption ratio between BR and point-to-point routing is

$$\frac{2P_2\frac{t}{2} + 2P_1\frac{t}{8}}{P_2 t} = 1 + \frac{P_1}{4P_2}$$

The ratio of total energy consumption along the entire route is

$$\frac{k(2P_2\frac{t}{2}) + (k+1)(P_1\frac{t}{8})}{kP_2 t} = 1 + \frac{(k+1)P_1}{8kP_2}$$

Fig. 10 plots the energy consumption ratio computed above, with $P2 = 100\mu$W, $d_1 = 5$dm, $\alpha = 0.1, d_2 = 50$dm; $k = [2, 4, 8, 12, 30, 50, 100]$ (each corresponding to a line in the figure). The energy consumption ratio decreases when P_1 is smaller, while the value of k doesn't have a great influence on the ratio. Overall, the extra power consumption overhead caused by BR is mostly below 20%, and further decreases to below 5% when $P_1/P_2 < 0.5$. Such a comprise can be well justified by the potential capacity gain of a factor of 2.
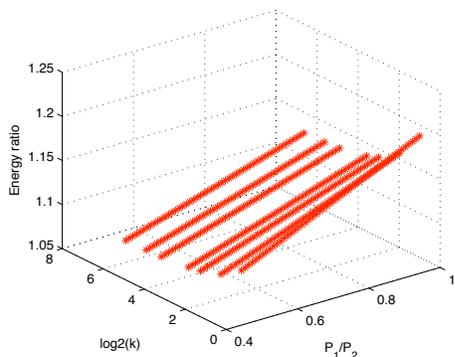
Fig. 10. Energy consumption ratio fo the entire unicast route: BR *vs* point-to-point routing.

IV. Buddy Routing: Unicast

In this section, we complete the design of a routing/MAC protocol suite, for applying Buddy Routing for unicast in multi-hop wireless networks consisting of extremely power constrained devices, as exampled by NanoNets and smart dust [9]. We describe the overall routing solution, as well as a tailored power and MAC optimization module in Sec. IV-A, and present simulation results in Sec. IV-B.

A. The BR Algorithms for Unicast

Table I presents the algorithms for BR unicast. Here r_b (radius of smallest circle in Fig. 11) is the maximum distance between a pair of buddy nodes, r_{min} (medium circle) and r_{max} (large circle) are the minimum and maximum allowed distances between two neighbor buddy pairs, respectively.

TABLE I

BR UNICAST ALGORITHMS: ROUTING & MAC OPTIMIZATION

1. Pair-to-pair greedy geographic unicast routing

find closest neighbor u of source
 $pair = \{source, u\}$
 while destination $\notin pair$ **do**
    if $dist(pair, destination) \leq r_{max}$:
       find closest neighbor v of destination
       $pair_{next} = \{destination, v\}$
    else:
       find $pair_{next}$, such that $r_{min} \leq dist(pair, pair_{next}) \leq r_{max}$
       and $dist(pair_{next}, destination)$ as small as possible
    end if
    PNC-based pair-to-pair packet transmission: $pair \rightarrow pair_{next}$
    $pair = pair_{next}$
 end while

2. Iterative MAC layer optimization

$\delta \leftarrow 1$
 while $\delta > \epsilon$:
    2.1. adjust time slot lengths in t_{11}, t_{12}, t_{13} and t_2
       — so that the capacity in each time slot is equal
    2.2. inter-pair power optimization
       — adjust P_2 of bottleneck long BR hop & neighbor pairs
       — achieve equal capacity at bottleneck link & 2 neibghbor links
    2.3. intra-pair power optimization
       — adjust P_1 in bottleneck short BR pair & neighbor pairs
       — achieve equal capacity at bottleneck pair & 2 neibghbor pairs
    — $\delta \leftarrow$ increment in end-to-end capacity due to 2.1-2.3
 end while

The idea behind BR unicast routing is to extend the well-known greedy geographical routing algorithm [8], which is known for its light-weight and fully distributed nature, form the point-to-point domain to the pair-to-pair domain. At each step in the iterative forwarding process, the algorithm looks for a next-hop pair between the two co-axial circles of radius d_3 and d_2, which is closest to the destination. The routing algorithm assumes a relatively dense network, such that the search for a buddy within a pair and the search for a next-hop pair of buddies can succeed. If the network density does not meet such a desired property, a hybrid route that combines pair-to-pair BR routing and traditional point-to-point routing can be resorted to.

We now take an overview of the complexity of the BR algorithms, for application in a NanoNet. The iterative power refinement is based on simple computation and neighbor communication only. The TDMA MAC is known for its low overhead, when compared to random access based protocols. The greedy geographical routing is stateless and of light weight. However, obtaining and maintaining location information at nanonodes may constitute a considerable overhead, if the NanoNet consists of mobile nodes. Our current design of BR is therefore more suitable for a relatively static network environment. Lastly, while the original proposal of PNC requires symbol level synchronization and accurate estimation of channel state information,

such requirements are relaxed in the latest developments of asynchronous physical layer network coding [12].
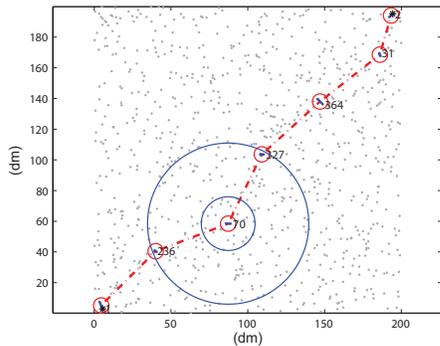
Fig. 11. BR unicast based on pair-to-pair greedy geographical routing.

Fig. 11 depicts a multi-hop unicast route found by the BR unicast routing algorithm. We have further enhanced the algorithm in Table I with a number of extra functionalities. First, in the case that the last pair of buddies in the BR route (excluding the destination pair) is too close to the destination, it will be discarded and replaced by a new pair with roughly equal distance to the destination and the previous pair. Second, we further implemented the planar face routing module [8] to enable the greedy geographic routing algorithm to be able to route around a large area void of wireless nodes, as shown in Fig. 12.
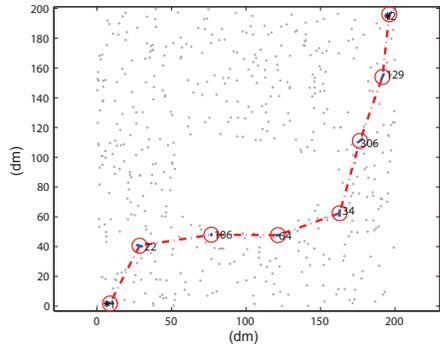
Fig. 12. BR unicast with Greedy Routing, with planar face routing implemented.

B. Simulation Results: BR Unicast

Fig. 13 depicts the effectiveness of the MAC optimization module in part 2 of Table I. In this set of simulations, 700 nodes are deployed in the network, each with maximum Tx power of 120μW. The end-to-end capacity of the BR route monotonically increases, and stabilizes after five rounds. The increment in each round is more or less random, and is not monotonic. End-to-end throughput is more than doubled after the iterative power/MAC optimization.

Fig. 14 compares the end-to-end throughput of BR with traditional point-to-point routing, both with and without MAC layer optimization, in networks of various sizes. The maximum power available for each node is 120μW. Each throughput is computed as the average of five executions of the routing algorithm in question, over different network topologies. We can see that throughput of buddy routing after optimization is almost twice of that of
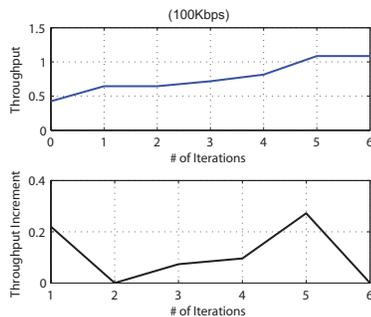
Fig. 13. BR Unicast. Top: throughput at each round. Bottom: throughput increase at each round. Note that the throughput improvement from round 1 to round 2, although very small, is not zero.
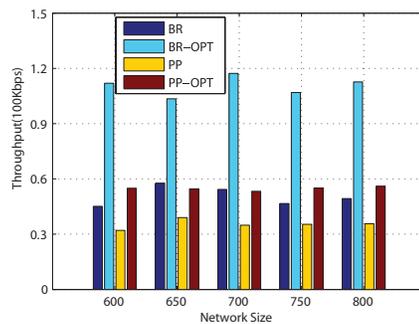
Fig. 14. BR Unicast, end-to-end throughput comparison, with varying network sizes.

point-to-point routing. The underlying reason for such a gain is simple yet fundamental: the BR gadget in Fig. 2 has twice the capacity of a point-to-point link, under equal nodal power budget. Such a significant gain in throughput can well justify the 5% to 20% overhead in power consumption observed in Sec. III-C.
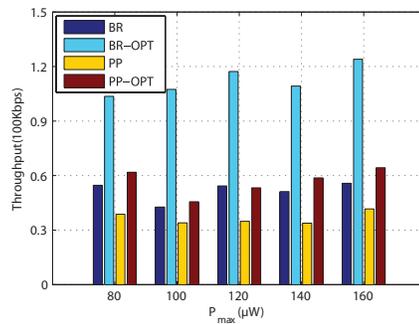
Fig. 15. BR Unicast, end-to-end throughput comparison, with varying maximum node power.

Fig. 15 shows a similar throughput comparison as in Fig. 14, with varying maximum node power instead of varying network sizes. A similar throughput gain is observed, which appears not sensitive to the choice of the maximum node power.

V. BUDDY ROUTING: MULTICAST

The pair-to-pair forwarding mechanism works well in a unicast path, which does not have branches. Multicast models a class of one-to-many data dissemination, where a common data

item of interest is to be transmitted to a group instead of a single destination, *e.g.*, along a multicast tree. For multi-hop multicast routing, a new challenge is to replicate a data packet from an upstream node pair to more than one pairs, for supporting branching in the multicast tree. A multicast branching gadget based on PNC has been designed accordingly. We introduce this multicast BR gadget in Sec. V-A, apply it to design BR multicast algorithms in Sec. V-B, and perform simulation evaluations in Sec. V-C.

A. The Multicast BR Gadget
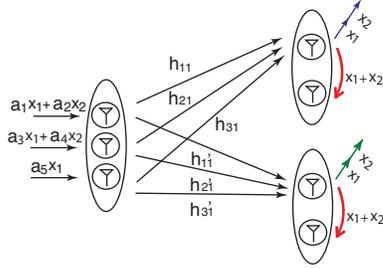
Fig. 16. PNC gadget for simultaneously group-to-multi-group transmission, for BR multicast.

As shown in Fig. 16, At each branching node, who has two downstream neighbor buddy pairs, we disseminate the data packet to three nodes in a collaborating group, two of which possessing the entire packet (x_1 and x_2), a third possessing half of the packet (x_1). Precoding is performed at each node as illustrated, such that the following signal alignment [7] at the top node of each node Rx pair is achieved:

$$\begin{cases} h_{11}a1 + h_{21}a_3 + h_{31}a_5 = h_{11}a_2 + h_{21}a_4 \\ h'_{11}a1 + h'_{21}a_3 + h'_{31}a_5 = h'_{11}a_2 + h'_{21}a_4 \end{cases}$$

For successfully align the perceived directions x_1 and x_2 at both the top and bottom pairs simultaneously, we need at least 5 precoding variables, for the two equations above to have solutions. Consequently, a 3-node group is required at each branching point in the multicast tree.

B. BR Algorithms: Multicast

The BR multicast algorithms are summarized in Table II. We design a two-tier solution, where a geometric multicast tree algorithm computes the multicast tree topology at the high level (Step 1), then the BR unicast algorithm from Table I is applied at each tree branch for data forwarding (Step 2). An iterative power/MAC optimization module (Step 3) then follows, similar to the unicast case.

The geometric Steiner tree algorithm starts by including two multicast terminals in the tree, then expands the tree one terminal at a time: a new terminal with shortest total distance to two terminals in the tree is selected, and connected using a local Steiner tree. The algorithm stops when all multicast terminals are covered by the tree. The algorithm guarantees that each node in the tree has degree at most 3, therefore the one-to-two branching capability of the multicast gadget in Fig. 16 is always sufficient.

Fig. 17 (one-to-three multicast) and Fig. 18 (one-to-two multicast) show the multicast trees built by the geometric Steiner tree

TABLE II
BR MULTICAST ALGORITHM STRUCTURE

1. Geometric Steiner tree construction
find closest receiver to s, t^*
$processed = \{s, t^*\}$
$active = T - \{t^*\}$
while $active \neq \{\}$:
pick t from $active, s.t.$ total distance from t
to two closest nodes in $processed$ is minimum
let u, v be the two closet nodes in $processed$ to t
connect t to u and v through the Fermat point
if u or v has degree 3: remove from $processed$ set
$active \leftarrow active - \{t\}; processed \leftarrow processed + \{t\}$
end while
2. For each edge in multicast tree built in 1:
for each node u in tree:
if degree of u is 2: identify pair
else: identify triple
apply BR unicast algorithms for routing between two ends.
3. Iterative MAC layer optimization

Fig. 17. BR Multicast with geometric tree construction, one-to-three multicast.

algorithm, in Step 1 of Table II. There are 950 nodes in Fig. 17, and 600 nodes in Fig. 18. A 2-node group is connected into a line segment, a 3-node group at each branching point is connected into a triangle.

The BR multicast algorithm also contains an iterative MAC optimization module, after routing is performed. Tx power and time slot lengths are adjusted for improving end-to-end multicast throughput. The operations here are similar to that in the unicast case. The main difference is that at a branching node group in the multicast tree, neighboring node pairs/triples along different branches of the tree are taken into consideration, when adjusting power and time slot lengths.

C. Simulation Results

Fig. 19 shows the end-to-end multicast throughput increase during each round of the MAC layer optimization. Three out of 900 nodes in the network are multicast terminals. The maximum power available at each node is 160μW. A similar trend to that in the unicast case is observed: the multicast throughput stabilizes after a small number of rounds. The multicast throughput monotonically increases during the optimization, although the amount of improvement in each round is not monotonic.

Fig. 20 shows the comparison of end-to-end multicast throughput between BR multicast and point-to-point multicast, both with and without MAC layer optimization. The maximum power
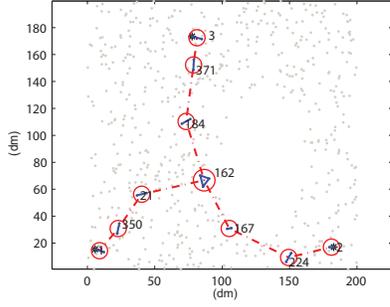
Fig. 18. BR Multicast with geometric tree construction, one-to-two multicast in a network with large void.
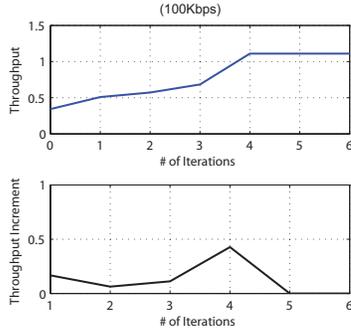
Fig. 19. BR Multicast. Top: throughput at each round. Bottom: throughput increase at each round.

available at each node is 160μW. The number of terminals is 3. Network size varies from 750 to 950 nodes. Each data point is the average of five simulation runs. We can see that the throughput of BR multicast is close to twice of that of point-to-point multicast, and that the MAC layer optimization significantly improves the achievable throughput, through (a) mitigating interference at bottleneck links, and (b) intelligently adjusting Tx time slot lengths. Achievable multicast throughput appears to slightly increase as the network size grows, since more nodes in the network implies better choices are possible for tree construction and node pair/triple formation.

Fig. 21 shows a similar comparison of multicast throughput, but under varying maximum Tx power instead of varying network size. The throughput of BR multicast is roughly, sometimes even higher than, twice of that of point-to-point routing. There
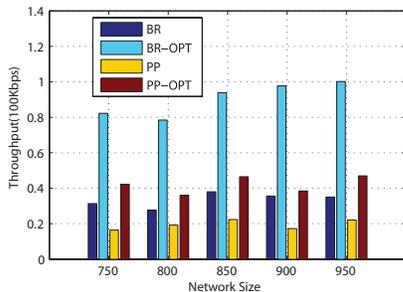
Fig. 20. BR multicast: end-to-end multicast throughput comparison with point-to-point schemes, under different network sizes.
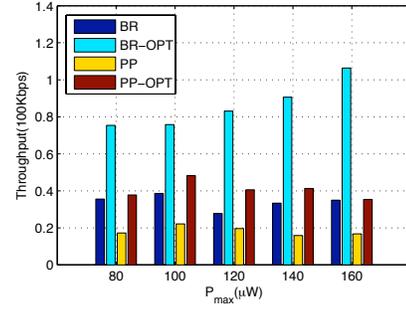
Fig. 21. BR multicast: end-to-end throughput comparison with point-to-point schemes, under different maximum Tx power.

are 900 nodes in the network, with three multicast terminals.
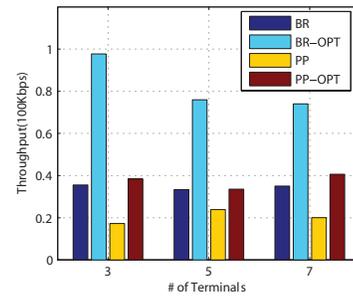
Fig. 22. BR Multicast, end-to-end throughput comparison with growing multicast group size.

Fig. 22 is throughput comparison with varying sizes of the multicast group. There are 900 nodes in this network. The maximum power available at each node is 160μW. An increase in the number of multicast receivers, in the same network environment, usually leads to a decrease in achievable multicast throughput, since the multicast tree involves more branches that incur more severe interference. Nonetheless, in each case, BR multicast can still manage to achieve roughly twice the throughput of point-to-point multicast.

VI. CONCLUSION

New wireless sensor networks with extremely small and power limited devices, exampled by the NanoNet, are envisioned to play an important role in our future lives. We proposed a new routing paradigm tailored for such type of networks, Buddy Routing. BR groups weak wireless nodes into groups for collaborative data forwarding, based on a recent technique of physical layer network coding. By paying a moderate price in energy efficiency (energy consumed in per bit end-to-end transmission), BR has a potential to break through the nodal power limit in NanoNets, substantially improving the unicast and multicast throughput, as verified by our theoretical analysis and simulation results.

REFERENCES

[1] I. Akyildiz and J. Jornet, "Electromagnetic wireless nanosensor networks," *Nano Communication Networks*, vol. 1, no. 1, pp. 3–19, 2010.
[2] K. Jensen, J. Weldon, H. Garcia, and A. Zettl, "Nanotube radio," *Nano letters*, vol. 7, no. 11, pp. 3508–3511, 2007.
[3] J. Weldon, K. Jensen, and A. Zettl, "Nanomechanical radio transmitter," *physica status solidi (b)*, vol. 245, no. 10, pp. 2323–2325, 2008.

[4] B. Atakan and O. Akan, "Carbon nanotube-based nanoscale ad hoc networks," *Communications Magazine, IEEE*, vol. 48, no. 6, pp. 129–135, 2010.

[5] I. Akyildiz, F. Brunetti, and C. Blázquez, "Nanonetworks: A new communication paradigm," *Computer Networks*, vol. 52, no. 12, pp. 2260–2279, 2008.

[6] S. Zhang, S. C. Liew, and P. P. Lam, "Physical-layer Network Coding," in *Proc. of ACM Mobicom*, 2006.

[7] R. Zhou, Z. Li, C. Wu, and C. Williamson, "Physical Layer Network Coding with Signal Alignment for MIMO Wireless Networks," in *the Proceedings of the 8th IEEE International Conference on Mobile Ad-hoc and Sensor Systems (MASS)*, 2011.

[8] B. Karp and H. T. Kung, "GPSR: Greedy Perimeter Stateless Routing for Wireless Networks," in *Proc. of ACM Mobicom*, 2000.

[9] J. M. Kahn, R. H. Katz, and K. S. J. Pister, "Mobile Networking for Smart Dust," in *Proc. of ACM Mobicom*, 1999.

[10] A. Ozgur, O. Leveque, and D. Tse, "Hierarchical Cooperation Achieves Optimal Capacity Scaling in Ad Hoc Networks," *IEEE Transactions on Information Theory*, vol. 53, no. 10, pp. 3549–3572, October 2007.

[11] C. Hu, X. Wang, D. Nie, and J. Zhao, "Multicast Scaling Laws with Hierarchical Cooperation," in *Proc. of IEEE INFOCOM*, 2010.

[12] L. Lu and S. C. Liew, "Asynchronous Physical-Layer Network Coding," *IEEE Transactions on Wireless Communications*, vol. 11, no. 2, pp. 819–831, February 2012.

[13] Y. Shi, Y. T. Hou, and J. Liu, "How to Correctly Use the Protocol Interference Model for Multi-hop Wireless Networks," in *Proc. of ACM Mobihoc*, 2009.